# FDTD ANALYSIS OF A DUAL-FREQUENCY MICROSTRIP PATCH ANTENNA

**S. Gao**

School of Engineering
Northumbria University
Newcastle Upon Tyne, UK

**L. W. Li**

Department of Electrical and Computer Engineering
National University of Singapore
Singapore

**A. Sambell**

School of Engineering
Northumbria University
Newcastle Upon Tyne, UK

**Abstract**—Characteristics of a single-layer, dual-frequency microstrip patch antenna, which uses a T-strip loaded rectangular microstrip patch, are studied. This antenna is easy to achieve good impedance matching at both frequencies by tuning the feed position and other design parameters. Another advantageous aspect is that it has high polarization purity. A detailed parameter study is performed and the theoretical analysis is based on the finite-difference time-domain (FDTD) method. The FDTD programs are developed and validated by measurement results. The effects of various antenna parameters on two resonant frequencies, frequency ratio, and radiation pattern characteristics of the antenna are analyzed and discussed. It is shown that various frequency ratios (1.5–2.49) can be obtained by varying the design parameters of this antenna. Similar radiation patterns with same polarization are obtained at two resonant frequencies. Several design curves are presented.

## 1. INTRODUCTION

Due to their inherent advantages of low profile, light weight, low cost, conformability, ease of fabrication and integration with RF devices, microstrip patch antennas have been widely employed in many practical applications for several decades [1–7]. Single-layer dual-frequency microstrip antenna with a single feed is urgently required in various radar and communications systems, such as synthetic aperture radar system, dual-band GSM/DCS 1800 mobile communications systems and Global Positioning System.

Generally, the dual-frequency microstrip antennas found in the literature may be divided into two categories, namely, multi-resonator antennas and reactive loading antennas. In the first kind of structures, the dual-frequency operation is achieved by means of multiple radiating elements, each supporting strong currents and radiation at its resonance. This category includes the multi-layer stacked-patch antennas using circular, annular, rectangular, and triangular patches [8–10]. A multi-resonator antenna in coplanar structures can also be fabricated by using aperture-coupled parallel microstrip dipoles [11]. As these antenna structures usually involve multiple substrate layers, they are of high cost. A large size is another drawback of the multi-resonator antenna, which makes it difficult for the antenna to be installed in hand-held terminals.

The reactive-loading microstrip patch antenna consists of a single radiating element in which the double resonant behavior is obtained by connecting coaxial [12] or microstrip stubs [13] at the radiating edges of a rectangular patch. This solution does not allow a frequency ratio higher than 1.2. Higher values of frequency ratio can be obtained by using two lumped capacitors connected from the patch to the ground plane [14]. By using multiple shorting pins located symmetrically with respect to the patch axes, dual-band operations can also be realized, as shown in [15]. Another kind of reactive loading can be introduced by etching slots on a patch. The slot loading allows to strongly modify the resonant mode of a rectangular patch, particularly when the slots cut the current lines of the unperturbed mode. In [16], it is shown that the simultaneous use of slots and short- circuit vias allows to obtain a frequency ratio from 1.3 to 3 depending on the number of vias. Dual-frequency operation of the microstrip antenna with a spur-line filter embedded in the patch has also been reported in [17] where a frequency ratio of $\sim 2.0$ between the two operating frequencies is shown. In such a dual-frequency scheme, the lower and higher operating frequencies are designed, respectively, at the resonant frequencies of a new resonant mode, generated by the perturbation of the embedded spur-line filter in the patch, and the $TM_{01}$ mode. Dual slot-loaded microstrip antenna with dual-frequency operation has been reported in [18, 19], where two parallel narrow slots are etched in the rectangular patch close to its radiating edges. The two slots are chosen to be close to the length of the radiating edge. In the case, the radiating characteristics of the antenna operating at the perturbed $TM_{01}$ and $TM_{03}$ modes are similar and have parallel polarization planes. Other dual-frequency antennas with slot loading or shorting-pin loading are reported in [20–22]. A single-layer, dual-frequency microstrip antenna is proposed in [23], which uses the rectangular microstrip patch loaded with T-shaped strips. A few experimental results are presented in [23]. This antenna is easy to achieve good impedance matching at two resonant frequencies using only a single probe feed. Experimental results of radiation patterns also demonstrate low cross-polarization levels (less than $-20$ dB) at both resonant frequencies, thus it is very promising for practical applications. For design purposes, more information about this kind of antenna is required, and a parametric study based on the full-wave method is still needed, which is the motivation of present paper.

In this paper, characteristics of the dual-frequency antenna proposed in [23] are studied in detail. The organization of this paper is as follows: Section 2 describes the finite-difference time-domain (FDTD) method used for numerical analysis and its validation by
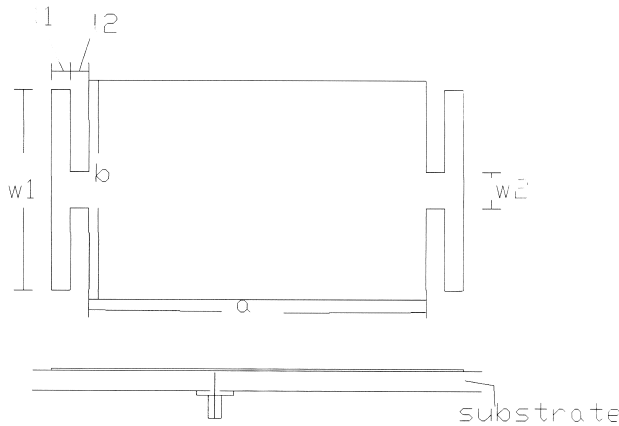
**Figure 1.** Configuration of the dual-frequency antenna.

comparisons between calculated and experimental results. Section 3 presents a numerical study illustrating the effects of various antenna parameters on the resonant frequencies, the frequency ratio, and radiation pattern characteristics of the antenna. The paper ends with conclusions in Section 4.

## 2. ANTENNA CONFIGURATION AND ANALYSIS METHOD

Figure 1 shows the configuration of the dual-frequency antenna. The antenna consists of a microstrip patch, supported on a grounded dielectric sheet of thickness $h$ and dielectric constant $\varepsilon_r$. The rectangular patch has a length of $a$ and a width of $b$. Two T-shaped strips are loaded at two radiating edges of the rectangular patch. The T-shaped strip is defined by parameters $l_1$, $w_1$, $l_2$ and $w_2$, as indicated in the figure. The feed point is located at the central line of the patch, with a distance of $d_f$ from the patch center.

### 2.1. Numerical Method of Analysis

In the numerical analysis of this antenna, we use the FDTD algorithm, because it is simple to understand and can be used to analyze antennas of complex structures. As the detailed theory on FDTD method is available in [24–28], only a brief outline will be presented here. The first step in designing an antenna with an FDTD code is to grid up the object. A number of parameters must be considered in order for the code to work successfully. The grid size must be small enough so

that the fields are sampled sufficiently to ensure accuracy. Once the grid size is chosen, the time step is determined such that numerical instabilities are avoided, according to the courant stability condition.

A Gaussian pulse voltage with unit amplitude, given by

$$V(t) = e^{-\frac{(t-t_0)^2}{T^2}} \tag{1}$$

where $T$ denotes the period and $t_0$ identifies the center time, is excited in the probe feed. For the feed probe, we use a series resistor $R_s$ with the voltage generator to model the current in the feed probe [21, 27]. To truncate the infinite space, a combination of the Liao's third-order absorbing boundary conditions and the super-absorbing technique is applied, as in [21, 25–27]. After the final time-domain results are obtained, the current and voltage are transformed to those in the Fourier domain. The input impedance of the antenna is then obtained from the

$$Z_{in} = \frac{V(f)}{I(f)} - R_s \tag{2}$$

The results of input impedance are then used to obtain the return loss characteristics of the antenna. To get the radiation pattern characteristics, a sinusoidal excitation at probe feed is used, which is given by

$$V(t) = \sin(2\pi f_0 t) \tag{3}$$

where $f_0$ denotes the resonant frequency of interest. The field distributions are recorded at one instant of time after the steady state has been reached. In our analysis, the total time for stability is more than 6 cycles. After the field distribution has been obtained, the radiation pattern can be readily calculated by using the near-field to far-field transformation [21, 28].

## 2.2. Comparisons between Calculated Results and Experimental Results

Based on the FDTD algorithm described previously, a software program in Fortran 77 language has been developed by us. To verify the FDTD code, we made a lot of simulations and comparisons are made among many sets of theoretical results and measured results. Here, due to the limited space, only one example is shown subsequently.

The experimental results in [23] are used here for validation of our FDTD analysis. The antenna parameters are: $a = 36\,\text{mm}$, $b = 40\,\text{mm}$, $l_1 = 3\,\text{mm}$, $w_1 = 40\,\text{mm}$, $l_2 = 1\,\text{mm}$, $w_2 = 6\,\text{mm}$, $\varepsilon_r = 4.26$,
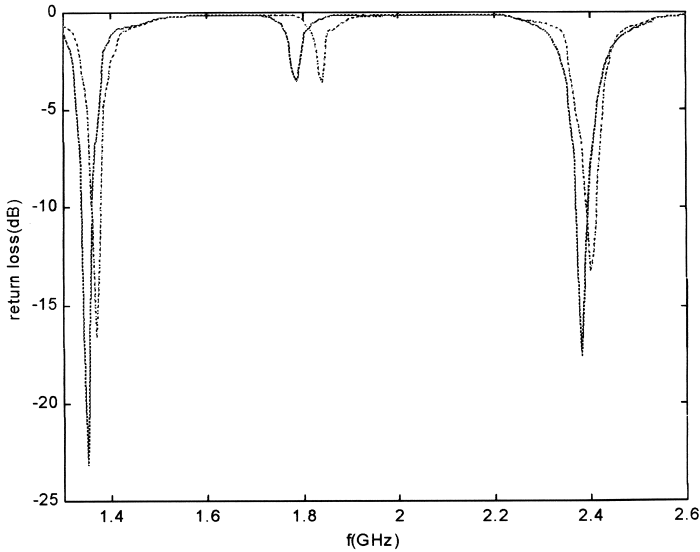
**Figure 2.** Measured and calculated results of return loss. Measured results: solid line; calculated results: dashed line.

$h = 1.6 \, \text{mm}$. The measured results of return loss are presented in Figure 2, together with the calculated results by using our FDTD programs. The two Resonance are found at 1370 MHz and 2400 MHz, respectively, as expected. The agreement between the measured and calculated results is fairly well, which validates our FDTD programs. Some of other comparisons are also available in [21, 26]. Generally, we observe a good agreement between these results. In the following, a parameter study of the dual-frequency microstrip patch antenna will be performed using the FDTD code.

The practical designs of this antenna will be based on full-wave simulation tools, and need some cut and try. To start the design, all suitable parameters are given as an initial condition to obtain the input impedance locus in the Smith Chart. Once the individual locus corresponding to its 1st and 3rd resonant frequencies in the Smith Chart is known, a suitable feeding location can be achieved by applying a general rule of tuning the input impedance of the patch antenna. As we know, the $TM_{30}$ mode at 3rd resonant frequency is perturbed more seriously than $TM_{10}$ mode at the 1st resonant frequency by T-strip loading, the width can be adjusted so as to obtain better matching for the 3rd resonant frequency. Finally, frequency is scaled to fit its physical dimension.

## 3. NUMERICAL RESULTS

### 3.1. Effects of $\varepsilon_r$

Based on the FDTD code, a lot of numerical simulations of the T-strip loaded, rectangular patch antenna have been performed by us. According to these results, Figure 3(a) shows the two resonant frequencies of $f_{01}$ and $f_{03}$ for the perturbed $TM_{01}$ and $TM_{03}$ modes against $\varepsilon_r$. In the calculation, other parameters of the $T$-strip loaded, rectangular patch are fixed as: $a = 36\,\mathrm{mm}$, $b = 40\,\mathrm{mm}$, $l_1 = 3\,\mathrm{mm}$, $w_1 = 40\,\mathrm{mm}$, $l_2 = 1\,\mathrm{mm}$, $w_2 = 6\,\mathrm{mm}$, $h = 1.6\,\mathrm{mm}$. It is shown that with the increase of $\varepsilon_r$ the resonant frequencies at both the $TM_{01}$ and $TM_{03}$ modes decrease accordingly. When the value of $\varepsilon_r$ equals to 1.0, the frequencies $f_{01}$ and $f_{03}$ reach the maximum values of 2.61 and 4.53 GHz, respectively. The resonant frequencies $f_{01}$ and $f_{03}$ reach the values of 1.37 and 2.4 GHz, respectively, when the value of $\varepsilon_r$ is increased to 4.26.

The variation of frequency ratio between two resonant frequencies with respect to $\varepsilon_r$ is presented in Figure 3(b). In this calculation, other parameters of the antenna are fixed as those in Fig. 3(a). The frequency ratio shows only a very slight variation with the increase of $\varepsilon_r$. In the present case, the frequency ratio varies in the range between 1.76 and 1.78.

As there are a lot of design parameters for this antenna (the width and length of patch, four design parameters of $T$-shaped strip, and feed positions, etc), good impedance matching at both frequencies can be obtained by tuning these parameters appropriately. To illustrate this point, Figure 4 gives the return loss of three antennas with different $\varepsilon_r$ Good impedance matching is obtained at 1.37 GHz and 2.4 GHz, respectively in the case of $\varepsilon_r$ equal to 4.26. When $\varepsilon_r$ is decreased to 2.33, again we observe good impedance matching at 1.83 GHz and 3.24 GHz, respectively. Furthermore, when $\varepsilon_r$ is reduced to 1.0, good impedance matching is achieved at 2.61 GHz and 4.53 GHz, respectively. In the three cases, $d_f$ is fixed as 9 mm. However, in many cases, the feed position needs to be adjusted for good impedance matching at both frequencies. We also observe a dip in between the two resonance, which is due to the excitation of $TM_{02}$ mode. The excitation of other higher order modes is also observed for the cases of $\varepsilon_r$ equal to 4.26 and 2.33, as shown in the figure.

The radiation patterns of three antenna with different $\varepsilon_r$ at $f_{01}$ and $f_{03}$ are shown in Figures 5 and 6, respectively. Figure 5(a) shows the comparisons of $E$-plane radiation patterns among three antennas resonant at the $TM_{01}$ mode, where $\varepsilon_r$ is 4.26, 2.33 and 1.0, respectively Other antenna parameters are same as those in Figures 3.
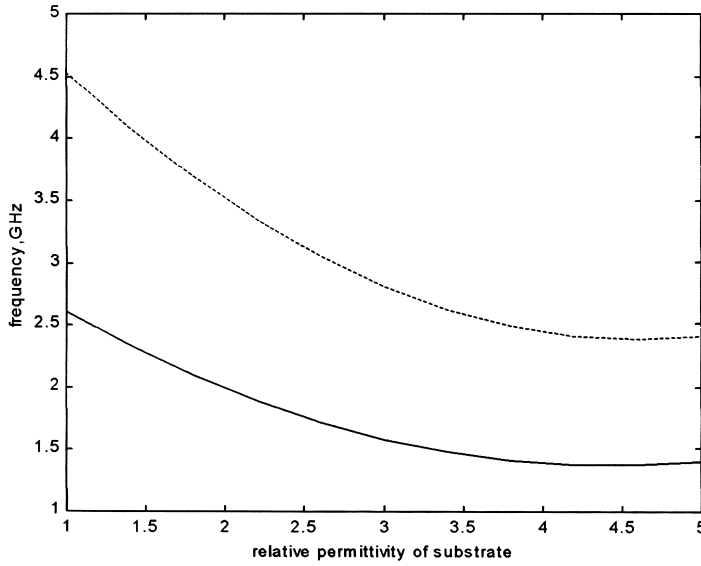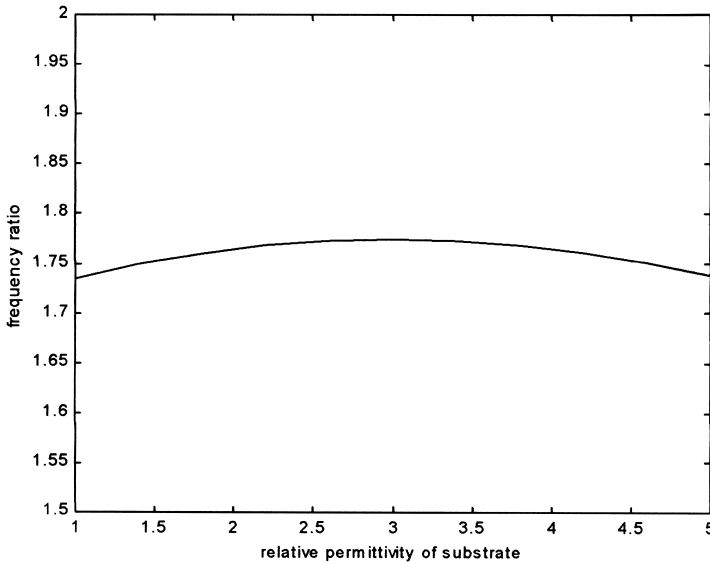
(a) Resonant frequencies versus $\varepsilon_r$



(b) Frequency ratio versus $\varepsilon_r$

**Figure 3.** Resonant frequencies and frequency ratio versus $\varepsilon_r$, $f_{01}$: solid line; $f_{03}$: dashed line.
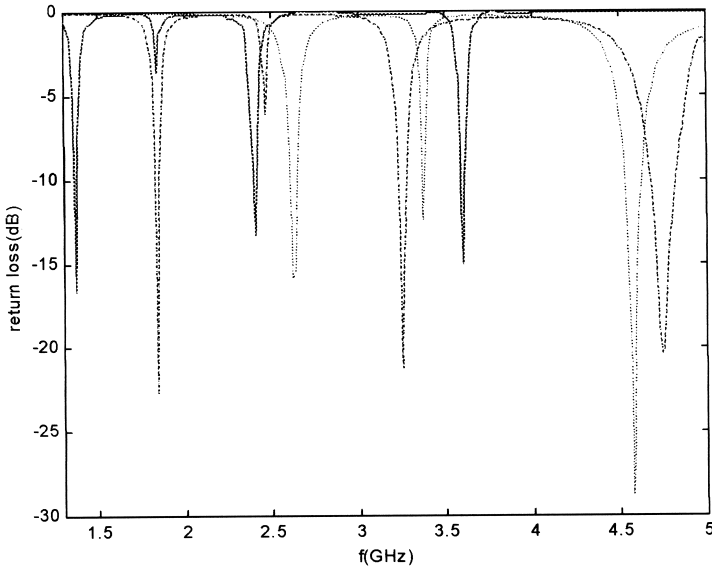
**Figure 4.** Return loss results for three antennas with different $\varepsilon_r$, $\varepsilon_r = 4.26$: solid line; $\varepsilon_r = 2.33$: dashed line; $\varepsilon_r = 1.0$: dotted line.

These patterns are calculated at $1.37\,\text{GHz}$, $1.83\,\text{GHz}$ and $2.61\,\text{GHz}$, respectively. It is seen that the $E$-plane radiation pattern at $f_{01}$ is broadened with the increase of $\varepsilon_r$. The $H$-plane patterns at $f_{01}$ of the antennas with different $\varepsilon_r$ also show a tendency of slight broadening with the increase of $\varepsilon_r$ as shown in Figure 5(a). Figure 6 shows the comparisons of radiation patterns among three antennas resonant at the $TM_{03}$ mode. These patterns are calculated at $2.4\,\text{GHz}$, $3.24\,\text{GHz}$ and $4.53\,\text{GHz}$, respectively. It is seen that the radiation patterns at both $E$ plane and $H$ plane are broadened significantly when $\varepsilon_r$ increases. It is to be noted that these patterns at $f_{01}$, and $f_{03}$ are of same polarization.

## 3.2. Effects of $w_1$

Figure 7(a) shows the frequencies $f_{01}$ and $f_{03}$ against $\frac{w_1}{b}$. The variation of frequency ratio against $\frac{w_1}{b}$ is presented in Figure 7(b). It can be seen that, with the increase in $w_1$, two resonant frequencies decrease while the frequency ratio increases. When $\frac{w_1}{b}$ increases from 0.7 to 2 (i.e., $w_1$ increases from $28\,\text{mm}$ to $80\,\text{mm}$ in this case), the frequency $f_{01}$ decreases from $2.12\,\text{GHz}$ to $1.14\,\text{GHz}$ and the frequency $f_{03}$ decreases
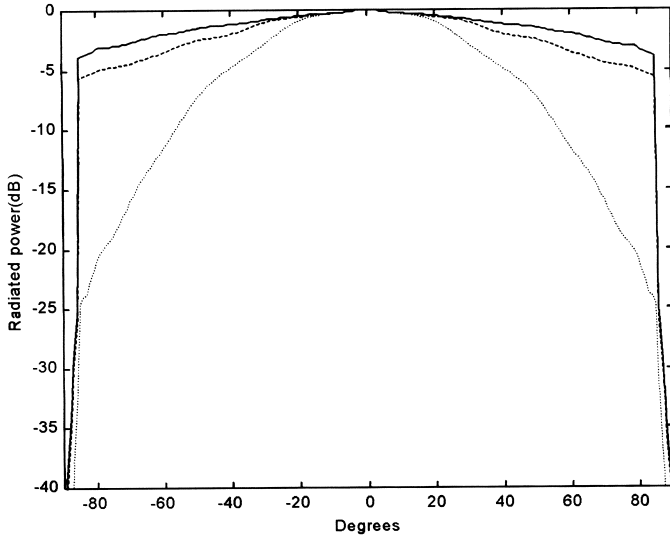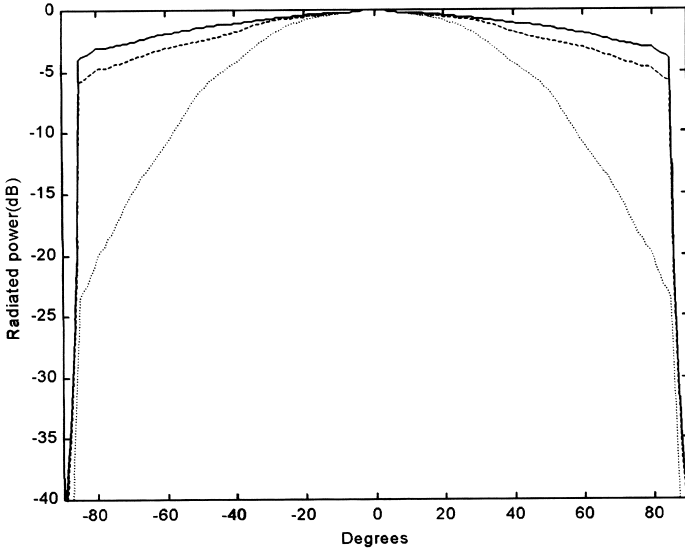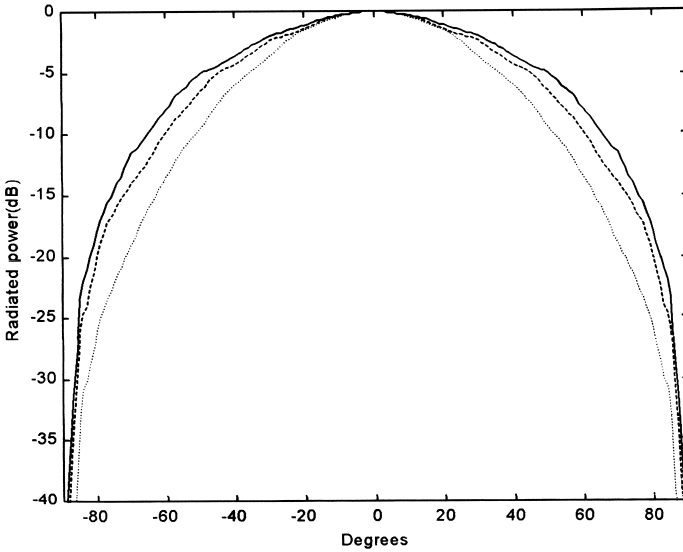
(a) E plane
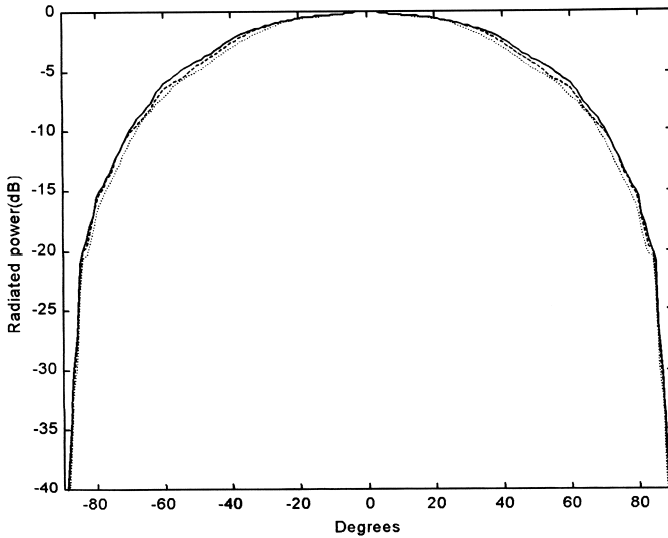


(b) H plane

**Figure 5.** Radiation patterns of three antennas at $f_{01}$, $\varepsilon_r = 4.26$: solid line; $\varepsilon_r = 2.33$: dashed line; $\varepsilon_r = 1.0$: dotted line.

(a) E plane



(b) H plane

**Figure 6.** Radiation patterns of three antennas at $f_{03}$, $\varepsilon_r = 4.26$: solid line; $\varepsilon_r = 2.33$: dashed line; $\varepsilon_r = 1.0$: dotted line.
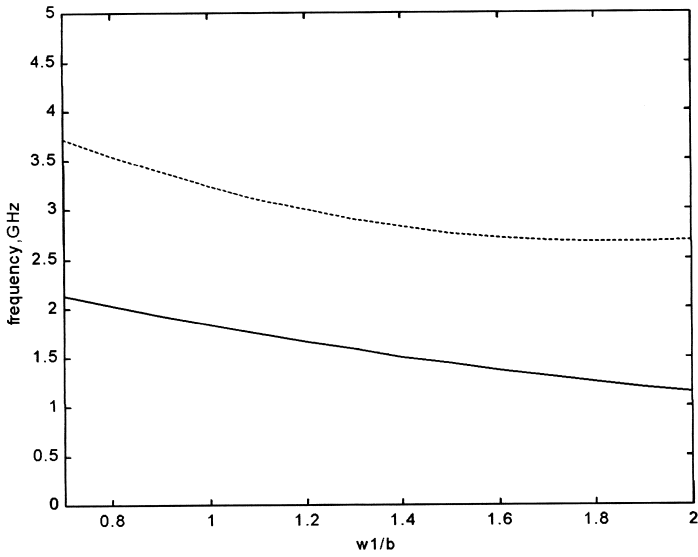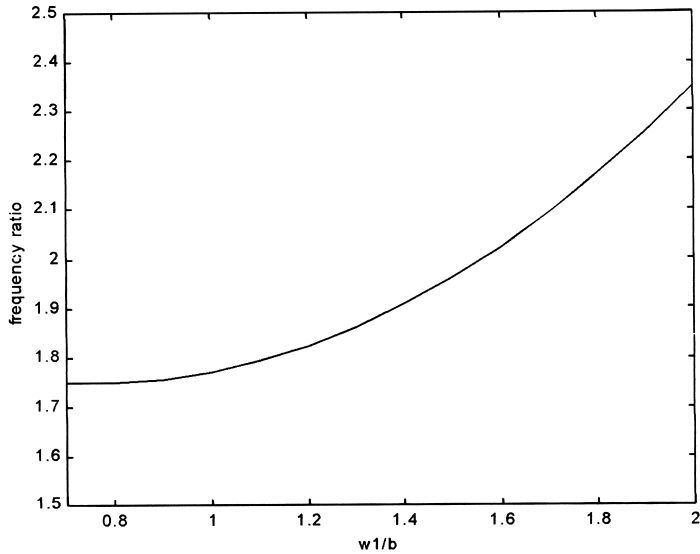
(a) Resonant frequencies versus $w_1/b$



(b) Frequency ratio versus $w_1/b$

**Figure 7.** Resonant frequencies and frequency ratio versus $w_1$, $f_{01}$: solid line; $f_{03}$: dashed line.

from $3.72\,\text{GHz}$ to $2.68\,\text{GHz}$. During this process, the frequency ratio increases monotonically from 1.75 to 2.35. In the calculation, other parameters are fixed as: $a = 36\,\text{mm}$, $b = 40\,\text{mm}$, $l_1 = 3\,\text{mm}$, $l_2 = 1\,\text{mm}$, $w_2 = 6\,\text{mm}$, $\varepsilon_r = 2.33$, $h = 1.6\,\text{mm}$.

The radiation patterns of three antenna with different $\frac{w_1}{b}$ at frequencies $f_{01}$, and $f_{03}$ are also studied, but the figures are omitted here for brevity. Similar radiation patterns with same polarization are obtained at two resonant frequencies. It is observed that at the $TM_{01}$ mode, the $E$-plane radiation patterns are broadened, while $H$-plane patterns show little differences when $w_1$ is increased from $28\,\text{mm}$ to $40\,\text{mm}$ and then $80\,\text{mm}$, respectively. At the $TM_{03}$ mode, the $E$-plane radiation patterns are narrowed, while the $H$-plane patterns are broadened when $w_1$ is increased. At first glance, it seems that further tuning of the resonant frequencies or radiation patterns may be possible if we decrease the value of $w_1$ further. However, from the calculated results, we note that a deformation in the $E$-plane patterns at $f_{03}$ will be resulted (i.e., a shift of the maximum radiation away from zero degree), when $\frac{w_1}{b}$ is less than 0.7 in this case.

### 3.3. Effects of $l_1$

The frequencies $f_{01}$ and $f_{03}$ versus $l_1$ are presented in Figure 8(a). It is shown that, with the increase of $l_1$, both the two resonant frequencies decrease accordingly, and $f_{03}$ decreases much slower than $f_{01}$. When the value of $l_1$, equals to $1.0\,\text{mm}$, the frequencies $f_{01}$ and $f_{03}$ reach the maximum values of 2.18 and $3.28\,\text{GHz}$, respectively. The resonant frequencies $f_{01}$ and $f_{03}$ reach the values of 1.28 and $3.18\,\text{GHz}$, respectively, when the value of $l_1$, is increased to $10\,\text{mm}$. In the calculation, other parameters are fixed as: $a = 36\,\text{mm}$, $b = 40\,\text{mm}$, $w_1 = 40\,\text{mm}$, $l_2 = 1\,\text{mm}$, $w_2 = 6\,\text{mm}$, $\varepsilon_r = 2.33$, $h = 1.6\,\text{mm}$.

The variation of frequency ratio with respect to $l_1$ is presented in Figure 8(b). In this calculation, other parameters of the antenna are fixed as those in Fig. 8(a). The frequency ratio shows a trend of quick increase with the increase in $l_1$. When the value of $l_1$ is increased from $1\,\text{mm}$ to $10\,\text{mm}$, the frequency ratio increases from 1.5 to 2.49.

The radiation patterns are also calculated. Similar radiation patterns with same polarization are obtained at two resonant frequencies. It is observed that at the $TM_{01}$ mode, the $E$-plane radiation patterns are slightly broadened, while $H$-plane patterns show little differences when $l_1$ is increased from $1\,\text{mm}$ to $3\,\text{mm}$ and then $10\,\text{mm}$, respectively. At the $TM_{03}$ mode, the $E$-plane radiation patterns are slightly broadened, while the $H$-plane patterns are slightly narrowed with the increase of $l_1$.
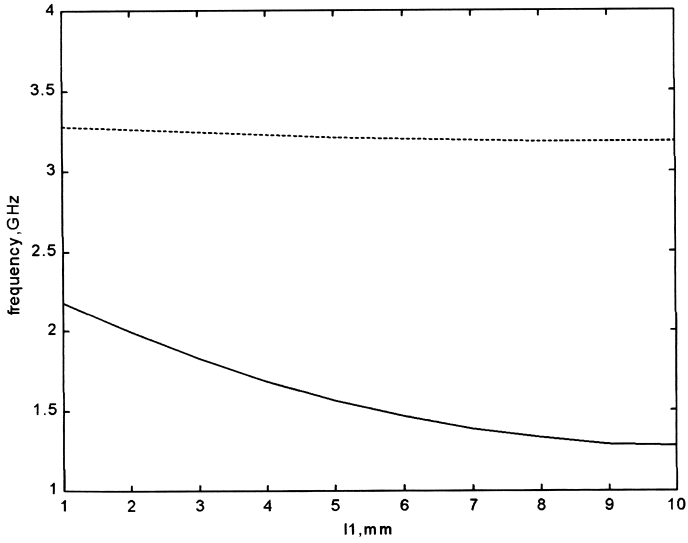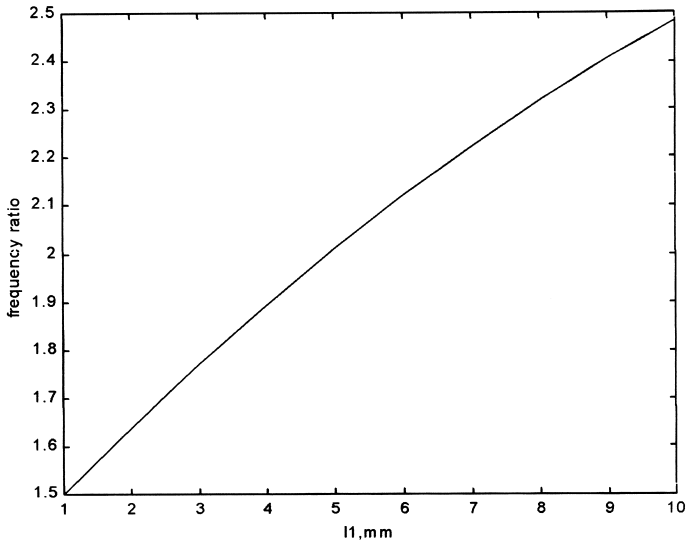
(a) Resonant frequencies versus $l_1$



(b) Frequency ratio versus $l_1$

**Figure 8.** Resonant frequencies and frequency ratio versus $l_1$, $f_{01}$: dashed line; $f_{03}$ solid line.

### 3.4. Effects of $w_2$

Figure 9(a) presents the frequencies $f_{01}$ and $f_{03}$ versus $w_2$. It is shown that, with the increase of $w_2$, the two resonant frequencies increase, too. When the value of $\frac{w_2}{b}$ equals to 0.025 (ie., $w_2 = 1$ mm), the frequencies $f_{01}$ and $f_{03}$ reach the values of 1.64 and 2.98 GHz, respectively. When the value of $\frac{w_2}{b}$ increases to 0.3 (i.e., $w_2 = 12$ mm), the frequencies $f_{01}$ and $f_{03}$ reach the values of 1.98 and 3.6 GHz, respectively. In the calculation, other parameters are fixed as: $a = 36$ mm, $b = 40$ mm, $l_1 = 3$ mm, $w_1 = 40$ mm, $l_2 = 1$ mm, $\varepsilon_r = 2.33$, $h = 1.6$ mm.

The variation of frequency ratio with respect to $w_2$ is presented in Figure 9(b). In this calculation, other parameters of the antenna are fixed as those in Fig. 9(a). The frequency ratio shows only a slight variation between 1.77 and 1.82 with the value of $\frac{w_2}{b}$ changing from 0.025 to 0.3.

From the calculated results of radiation patterns, we observe that at the $TM_{01}$ mode, both the $E$-plane and $H$-plane radiation patterns shows little variation, when $w_2$ is increased from 1 mm to 6 mm and then 12 mm, respectively. At the $TM_{03}$ mode, the $E$-plane radiation patterns are broadened, while the $H$-plane patterns are narrowed when $w_2$ is increased. It is to be noted that $w_2$ cannot be increased too much. From the calculated results, we observe that a deformation in the $E$-plane patterns at $f_{03}$ will be resulted, when $\frac{w_2}{b}$ is larger than 0.3 in this case.

### 3.5. Effects of $l_2$

The frequencies $f_{01}$ and $f_{03}$ versus $l_2$ are presented in Figure 10(a). It is shown that with the increase of $l_2$, the two resonant frequencies decrease. When the value of $l_2$ equals to 1 mm, the frequencies $f_{01}$ and $f_{03}$ reach the values of 1.83 and 3.24 GHz, respectively. When the value of $l_2$ increases to 10 mm, the frequencies $f_{01}$ and $f_{03}$ reach the values of 1.34 and 2.9 GHz, respectively. In the calculation, other parameters of the antenna are fixed as: $a = 36$ mm, $b = 40$ mm, $l_1 = 3$ mm, $w_1 = 40$ mm, $w_2 = 6$ mm, $\varepsilon_r = 2.33$, $h = 1.6$ mm.

The variation of frequency ratio with respect to $l_2$ is presented in Figure 10(b). In this calculation, other parameters of the antenna are fixed as those in Fig. 10(a). The frequency ratio increases from 1.77 to 2.165 with the value of $l_2$ changing from 1 mm to 10 mm.

According to the results of radiation patterns, we observe that at the $TM_{01}$ mode, the $E$-plane radiation patterns are slightly broadened, while $H$-plane patterns show little differences when $l_2$ is increased from 1 mm to 5 mm and then 10 mm, respectively. At the $TM_{03}$ mode, both the $E$-plane patterns and the $H$-plane patterns are slightly broadened
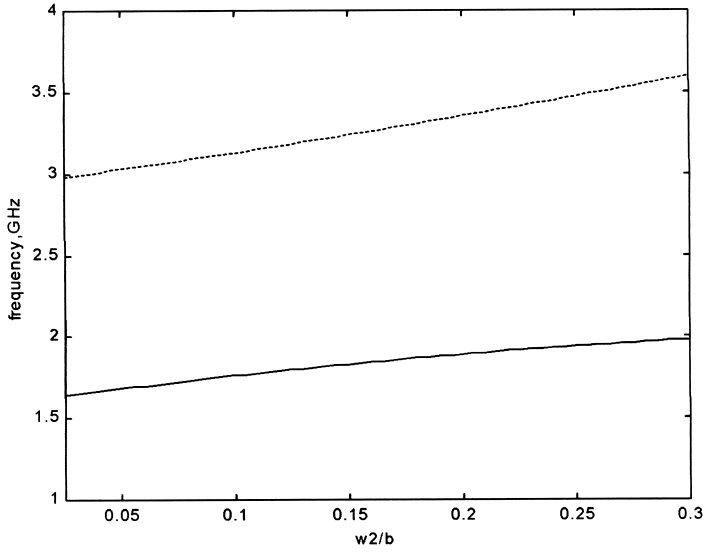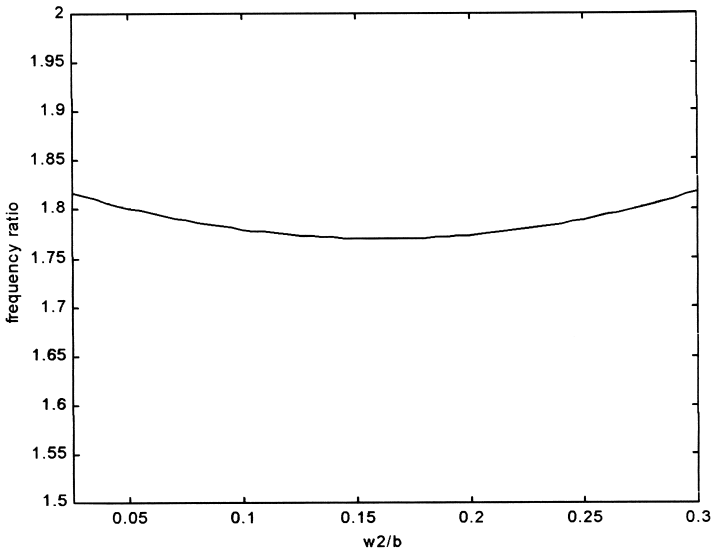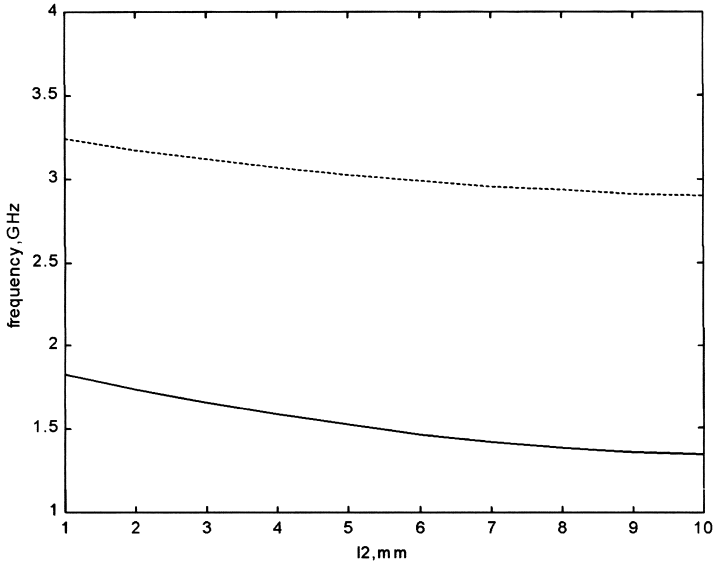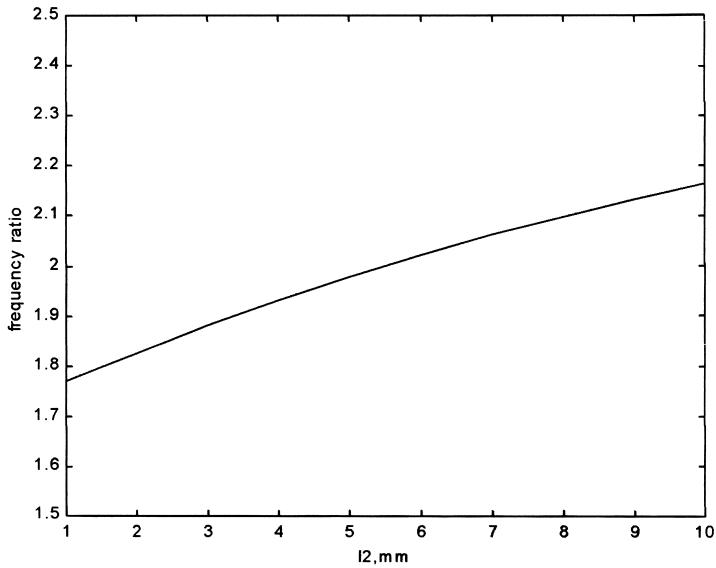
(a) Resonant frequencies versus $w_2$



( b) Frequency ratio versus $w_2$

**Figure 9.** Resonant frequencies and frequency ratio versus $w_2$, $f_{01}$: solidline; $f_{03}$: dashedline.

(a) Resonant frequencies versus $l_2$



(b) Frequency ratio versus $l_2$

**Figure 10.** Resonant frequencies and frequency ratio versus $l_2$, $f_{01}$: solid line; $f_{03}$ dashed line.

with the increase of $l_2$.

## 3.6. Effects of $a$

In Figure 11(a), the frequencies $f_{01}$ and $f_{03}$ versus $a$ are presented. It is shown that, with the increase of $a$, the two resonant frequencies decrease quickly. When the value of a equals to 30 mm, the frequencies $f_{01}$ and $f_{03}$ reach the values of 1.98 and 3.6 GHz, respectively. When the value of a increases to 48 mm, the frequencies $f_{01}$ and $f_{03}$ reach the values of 1.6 and 2.84 GHz, respectively. In the calculation, other parameters are fixed as: $b = 40$ mm, $l_1 = 3$ mm, $w_1 = 40$ mm, $l_2 = 1$ mm, $w_2 = 6$ mm, $\varepsilon_r = 2.33$  $h = 1.6$ mm.

The variation of frequency ratio with respect to a is presented in Figure 11(b). In this calculation, other parameters of the antenna are fixed as those in Fig. 10(a). The frequency ratio shows a slight variation between 1.77 and 1.82, with the value of $a$ changing from 28.8 mm to 50.4 mm.

As to the radiation patterns, it is shown that at the $TM_{01}$ mode, both the $E$-plane and $H$-plane radiation patterns show little variation, when a is increased from 28.8 mm to 50.4 mm. At the $TM_{03}$ mode, both the $E$-plane radiation patterns and the $H$-plane patterns are slightly broadened, when a is increased.

## 3.7. Effects of $h$

Figure 12 shows the two resonant frequencies and the frequency ratio versus $h$. It is observed that, with the increase of $h$, both the frequencies $f_{01}$ and $f_{03}$ increase slightly, and the frequency ratio increases slightly, too. When $h$ is 0.8 mm, a frequency ratio of 1.768 is obtained and the $f_{01}$ and $f_{03}$ are 1.81 GHz and 3.2 GHz, respectively. The frequency ratio is increased to 1.772 and the frequencies $f_{01}$ and $f_{03}$ are 1.84 GHz and 3.26 GHz, respectively, when $h$ is 4.8 mm. In the calculation, other parameters of the T-strip loaded, rectangular patch are fixed as: $a = 36$ mm, $b = 40$ mm, $l_1 = 3$ mm, $w_1 = 40$ mm, $l_2 = 1$ mm, $w_2 = 6$ mm, $\varepsilon_r = 2.33$.

The radiation patterns are also calculated. Similar radiation patterns with same polarization are observed at two resonant frequencies. It is shown that at both the $TM_{01}$ and the $TM_{03}$ mode, all the radiation patterns are slightly narrowed, when $h$ is increased from 0.8 mm to 5 mm.

According to the above results, the frequency ratio can be trimmed by tuning $w_1$, $l_1$, and $l_2$. The behaviors in Figures 8 provide the present dual-frequency design with a tunable frequency-ratio range of 1.5–2.49.
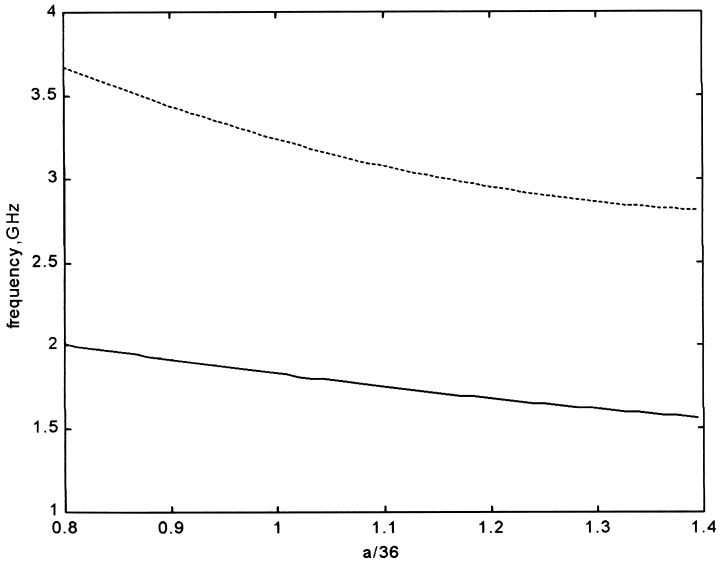
(a) Resonant frequencies versus $a$
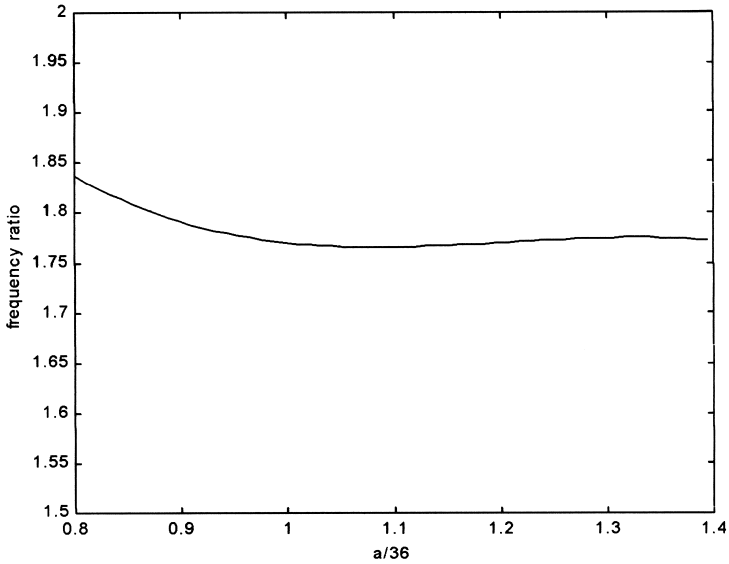
(b) Frequency ratio versus $a$

**Figure 11.** Resonant frequencies and frequency ratio versus $a$, $f_{01}$: solidline; $f_{03}$ dashedline.
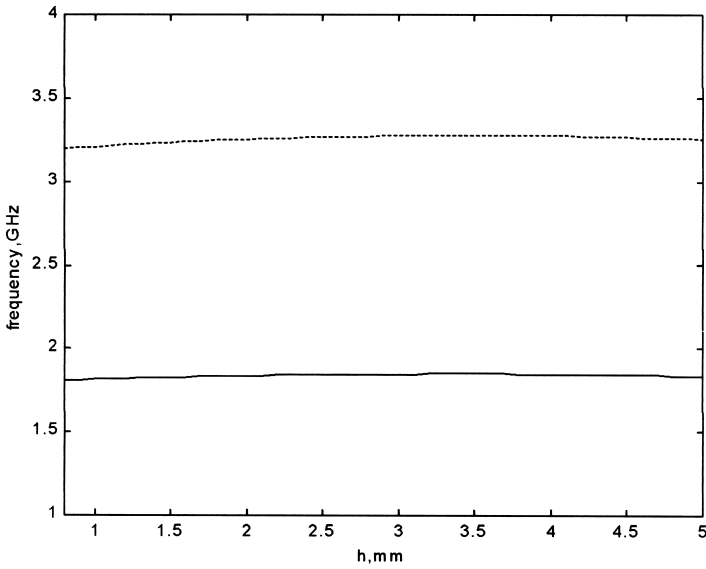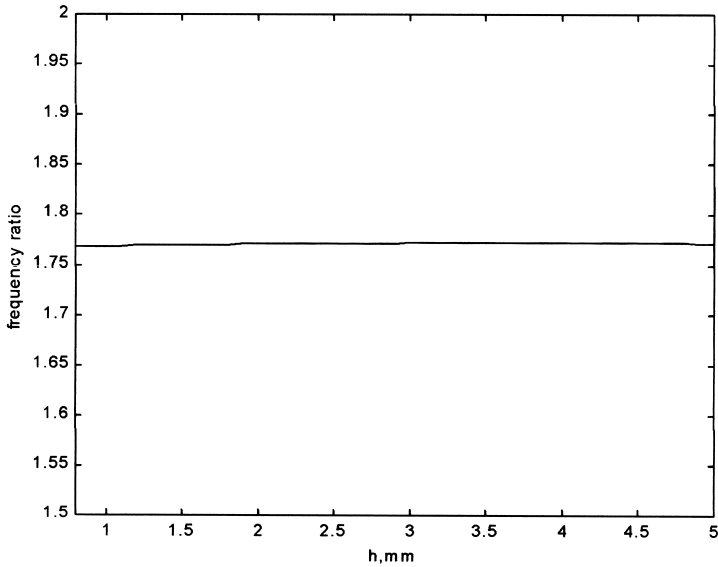
(a) Resonant frequencies versus $h$



(b) Frequency ratio versus $h$

**Figure 12.** Resonant frequencies and frequency ratio versus $h$, $f_{01}$: solid line; $f_{03}$ dashedline.

## 4. CONCLUSIONS

Based on the FDTD method, characteristics of a single-layer, dual-frequency microstrip antenna are studied in this paper. The FDTD code is developed and has been verified by measurement results. The variations of two resonant frequencies, the frequency ratio and radiation pattern characteristics with respect to several important antenna parameters, i.e., $\varepsilon_r$ (substrate permittivity), $a$, $l_1$, $w_1$, $l_2$, $w_2$ and $h$ are illustrated and discussed. It is shown that this dual-frequency antenna can obtain a frequency ratio in the range of 1.5 to 2.49. The frequency ratio can be trimmed by tuning $w_1$, $l_1$ and $l_2$. Similar radiation patterns with same polarization are obtained at two resonant frequencies. Both the $E$-plane radiation pattern and $H$-plane patterns at $f_{01}$ and $f_{03}$ are broadened with the increase of $\varepsilon_r$. Detailed numerical results are presented, which are helpful for practical antenna designs. These results are useful for understanding the behavior of the antenna when changing these design parameters. Compared with other techniques of realizing compact antenna, i.e., using high dielectric constant material or shorting-pin loading, the T-strip loaded, rectangular patch antenna has advantages of easy fabrication, low cost, high polarization purity and easiness of achieving good impedance matching at both frequencies by tuning the design parameters. This dual-frequency microstrip antenna is promising for many applications. By loading RF MEMS switches between the T strip and the rectangular patch, re-configurable dual-frequency antenna could be realized. The bandwidth could be broadened by using foam substrate.

## REFERENCES

1. James, J. R. and P. S. Hall (eds.), *Handbook of Microstrip Antennas,* Peter Peregrinus, UK, 1989.
2. Chang, K. (ed.), *Handbook of Mmicrowave and Optical Components,* Vol. 1, John Wiley & Sons, New York, 1989.
3. Bhartia, P., K. V. S. Rao, and R. S. Tomar, *Millimeter-Wave Microstrip and Printed-Circuit Antennas,* Artech House, Norwood, MA, 1991.
4. Pozar, D. M. and D. H. Schaubert (eds.), *Microstrip Antennas, the Analysis and Design of Microstrip Antennas and Arrays,* IEEE Press, New York, NY, 1995.
5. Gao, S. and S. S. Zhong, "Analysis and design of dual-polarized microstrip arrays," *International Journal of RF and Microwave CAE,* Vol. 9, No. 1, 42–48, 1999.

6. Gao, S. and S. S. Zhong, "Dual-polarized microstrip antenna array with high isolation fed by coplanar network," *Microwave and Optical Technology Letters,* Vol. 19, No. 3, 214–216, Oct. 1998.

7. Gao, S., "Dual-polarized microstrip antenna elements and arrays for active integration," Ph.D. thesis, Shanghai University Press, Shanghai, P. R. China, 1999.

8. Long, S. A. and M. D. Waton, "A dual-frequency stacked circular-disc antenna," *IEEE Trans.,* Vol. AP-27, No. 3, 281–285, 1979.

9. Dahele, J. S., K. F. Lee, and D. P. Wong, "Dual-frequency stacked annular-ring microstrip antenna," *IEEE Trans.,* Vol. AP-35, No. 11, 1281–1285, 1987.

10. Wang, J., R. Fralich, C. Wu, and J. Litva, "Multifunctional aperture-coupled stacked antenna," *Electron. Lett.,* Vol. 26, No. 25, 2067–2068, 1990.

11. Croq, F. and D. M. Pozar, "Multifrequency operation of microstrip antennas using aperture coupled parallel resonators," *IEEE Trans.,* Vol. AP-40, No. 11, 1367–1374, 1992.

12. Richards, W. F., S. E. Davidson, and S. A. Long, "Dual-band reactively loaded microstrip antenna," *IEEE Trans.,* Vol. AP-33, No. 5, 556–560, 1985.

13. Davidson, S. E., S. A. Long, and W. F. Richards, "Dual-band microstrip antenna with monolithic reactive loading," *Electron. Lett.,* Vol. 21, No. 21, 936–937, 1985.

14. Waterhouse, R. B. and N. V. Shuley, "Dual-frequency microstrip rectangular patches," *Electron. Lett.,* Vol. 28, No. 7, 606–607, 1992.

15. Hong, S. S. and Y. T. Lo, "Single-element rectangular microstrip antenna for dual- frequency operation," *Electron. Lett.,* Vol. 19, No. 8, 298–300, 1983.

16. Wang, B. F. and Y. T. Lo, "Microstrip antenna for dual-frequency operations," *IEEE Trans.,* Vol. AP-32, No. 9, 938–943, 1984.

17. Serrano-Vaello, A. and D. Sanchez-Hernandez, "Printed antennas for dual-band GSM/DCS 1800 mobile handsets," *Electronics Letters,* Vol. 34, No. 2, 140–141, 1998.

18. Maci, S., G. Avitabile, and G. Biffi Gentili, "Single-layer dual-frequency patch antenna," *Electronics Letters*, Vol. 29, No. 16, 1441–1443, 1993.

19. Maci, S., G. Biffi Gentili, P. Piazzesi, and C. Salvador, "Dual-band slot-loaded patch antenna," *IEEE Proc. Microw. Antennas Propag.,* Vol. 142, 225–232, June 1995.

20. Chen, W. S., "Single-feed dual-frequency rectangular microstrip

antenna with square slot," *Electronics Letters,* Vol. 34, No. 3, 231–232, 1998.

21. Gao, S. and J. Li, "FDTD analysis of a size-reduced, dual-frequency patch antenna," *Progress In Electromagnetics Research,* PIER 23, 59–77, 1999.

22. Wong, K. L. and W. S. Chen, "Compact microstrip antenna with dual-frequency operation," *Electronics Letters,* Vol. 33, No. 8, 646–647, 1997.

23. Deng, S. M., "A T-strip loaded rectangular microstrip patch antenna for dual-frequency operation," *IEEE Antennas and Propagation Symposium,* 940–943, 1999.

24. Yee, K. S., "Numerical solution of initial boundary value problems involving Maxwell's equations in isotropic media," *IEEE Trans.,* Vol. AP–14, 302–307, May 1966.

25. Liao, Z. P., H. L. Wong, G. P. Yang, and Y. F. Yuan, "A transmitting boundary for transient wave analysis," *Scientia Sinica,* Vol. 28, No. 10, 1063–1076, Oct. 1984.

26. Mei, K. K. and J. Fang, "Superabsorption — A method to improve absorbing boundary conditions," *IEEE Trans.,* Vol. AP-40, 1001–1010, Sept. 1992.

27. Gao, S. and J. Li, "FDTD analysis of serial corner-fed square patch antennas for single- and dual-polarized applications," *IEEE Proc. Microw. Antennas Propag.,* Vol. 146, 205–209, June 1999.

28. Gupta, K. C. and P. S. Hall (eds.), *Analysis and Design of Integrated Circuit-Antenna Modules,* John Wiley & Sons, Inc., New York, 2000.

**S. Gao** was born in 1972 in China, and received the Ph.D. in Microwave Engineering in 1999. He is currently a Senior Lecturer at Northumbria University, Newcastle Upon Tyne, UK. His research interests include the antenna design and modeling, numerical methods, high efficiency RF/Microwave power amplifiers, radio propagation, and communication systems.

**Le-Wei Li** received the B.Sc. degree in Physics from Xuzhou Normal University, Xuzhou, China, in 1984, the M.Eng.Sc. degree in Electrical Engineering from China Research Institute of Radiowave Propagation (CRIRP), Xinxiang, China, in 1987 and the Ph.D. degree in electrical engineering from Monash University, Melbourne, Australia, in 1992. In 1992, he worked at La Trobe University (jointly with Monash University), Melbourne, Australia as a Research Fellow. Since

1992, he has been with the Department of Electrical Engineering at the National University of Singapore where he is currently an Associate Professor. Since 1999, he has been also part-timely with High Performance Computation for Engineered Systems (HPCES) Programme of Singapore-MIT Alliance (SMA) as a SMA Fellow. His current research interests include electromagnetic theory, radio wave propagation and scattering in various media, microwave propagation and scattering in tropical environment, and analysis and design of antennas.

**A. Sambell** is currently a Professor and Dean of the School of Engineering and Technology, Northumbria University, Newcastle Upon Tyne, UK. His research interests include the design of microwave antennas for road-tolling and other applications.